Baroclinic Eddy Fluxes in a One-Dimensional Model of Quasi-geostrophic Turbulence*

R. LEE PANETTA

Joint Institute for the Study of the Atmosphere and Ocean, University of Washington, Seattle, Washington

ISAAC M. HELD

Geophysical Fluid Dynamics Laboratory/NOAA, Princeton University, Princeton, New Jersey

(Manuscript received 2 November 1987, in final form 16 May 1988)

ABSTRACT

Statistically steady states of a two-layer quasi-geostrophic model truncated to retain only the zonal mean flow and one nonzero zonal wavenumber, but with high meridional resolution, are described. The model is forced by imposing a time-mean unstable meridional temperature gradient, assuming that deviations from the time-mean are doubly periodic. A comparison is made with a more conventional channel model with the same zonal truncation, in which the flow is forced by radiative relaxation to an unstable temperature gradient. It is shown that the statistics of the channel model approach those of the doubly periodic model as the width of the unstable region in the former is increased. Implications for parameterization theories are discussed.

1. Introduction

It is difficult to test theories for baroclinic eddy fluxes against atmospheric observations. This is partly because complicating factors such as latent heat release and nonuniform lower boundary conditions are always present in the atmosphere but usually ignored in the theory, and partly because the atmosphere only allows one to test a theory over a limited parameter range. An attractive alternative is to test hypotheses against idealized dynamical models which are sufficiently simple that it is feasible to obtain a series of statistically steady states by numerical integration.

We study here what we believe to be the simplest model of a turbulent flow generated by baroclinic instability. It is a two-layer quasi-geostrophic model, "one-dimensional" in the sense that it is truncated to retain only the zonally averaged flow and one nonzero zonal wavenumber, but with high meridional resolution to allow for an enstrophy cascade. A time-mean flow consisting of an unstable uniform vertical shear is imposed, and the deviations from this time-mean flow are assumed to satisfy periodic boundary conditions in the meridional as well as zonal directions. Haidvogel and Held (1980, referred to hereafter as HH) used a similar two-layer doubly periodic model but with isotropic truncation in the horizontal. The present model is a further simplification of the model in HH which allows parametric investigations of statistically steady states that would be very costly using a model with isotropic truncation.

One cannot expect such a wave-mean flow interaction model to give a realistic representation of all phenomena occurring in two-dimensional turbulence. For example, small coherent vortices of the sort found by McWilliams (1984) cannot be produced. On the other hand, models with severe zonal truncation and high meridional resolution have proven useful in a number of meteorological contexts (Matsuno 1971; Geisler and Dickinson 1974; Holton 1971; Held and Suarez 1980). Haynes and McIntyre (1986) discuss the limitations as well as the successes of such models in studying the nonlinear evolution of critical layers. Furthermore, it is not obvious that the best route from this simplest of models to realistic atmospheric models passes through the isotropically truncated two-layer model; an alternative route is to proceed from the zonally truncated two-layer model to a zonally truncated model with realistic vertical structure, and *then* to an isotropically truncated model with realistic vertical structure.

In HH it is argued that the doubly periodic model can be thought of as a model of the interior of a channel flow forced in the more usual way by radiative relaxation to an unstable temperature gradient, in the limit that the width of the unstable region L is very much larger than a radius of deformation λ. This limit, in which it is argued that the eddy statistics become independent of L, can only exist if modes that span the

* Contribution No. 36, Joint Institute for the Study of the Atmosphere and Ocean.

Corresponding author address: Dr. R. Lee Panetta, Dept. of Meteorology, Texas A & M University, College Station, TX 77843.

unstable region are dynamically insignificant. If on the contrary the meridional scale of the dominant modes increases along with L, then one expects the time-averaged eddy energy to increase also, since larger eddies would be needed to produce the same eddy flux convergences and mean flow modification. Since the meridional scale of the most unstable linear mode generally does increase with increasing L, these most unstable modes must break up through secondary instabilities (e.g., Pedlosky 1975) into disturbances whose meridional structure scales with λ, if the statistics are to become independent of L.

The doubly periodic model addresses this issue in its most extreme form, for in such a model the most unstable wave has no meridional structure and does not modify the zonal mean flow at all. An initial condition with *only* this mode present results in continuous exponential growth. However, for general initial conditions HH find that the system does equilibrate and that the eddy statistics seem to be independent of the size of the doubly periodic domain. In HH it is argued that this independence is indirect evidence that the doubly periodic model does indeed approximate the flow in the interior of sufficiently wide channels.

The outline of this paper is as follows. The doubly periodic model truncated to one nonzero zonal wavenumber is described in section 2. Section 3 describes the statistically steady states of the model. We are able to show much more convincingly than in HH that the statistically steady states of such a model are independent of the size of the doubly periodic domain. The results also demonstrate that in spite of the severe spectral truncation, the spectral structure of the steady state is consistent with one's expectations for forced and damped quasi-geostrophic turbulence. The dependence of the domain-averaged heat (or buoyancy) flux on the various physical and computational parameters of the model is examined. Section 4 contains the central result of the paper. A channel model with the same zonal truncation is forced by radiative relaxation to a temperature gradient that is unstable in a central latitude belt. It is shown that the statistical behavior in the unstable belt converges to that of the doubly periodic model, as the width of the belt increases. In showing this, we focus on the zonally averaged potential vorticity flux, as knowledge of this quantity is all that is needed for closure in quasi-geostrophic models with linear nonconservative terms. The discussion in section 5 summarizes our main findings, and touches on the generation of long-lasting multiple-jet structures in both the channel and doubly periodic models.

2. The doubly periodic model

The fluid layers are of equal resting depth H, and are bounded above and below by rigid horizontal surfaces. The meridional coordinate y measures distance from the center of the domain, where the Coriolis parameter is f_0. Subscripts 1 and 2 index properties of the upper and lower layers, respectively. In terms of the layer densities ρ_i, the Rossby radius λ is defined by $\lambda^2 = g(\rho_2 - \rho_1)H/(2\rho_2 f_0^2)$. We include a thermal damping, lower Ekman friction, and a scale-selective biharmonic diffusion of vorticity to absorb the enstrophy cascade. In terms of the total streamfunctions Ψ_j, the dimensional equations for quasi-geostrophic motion on a β-plane are

$$\partial Q_1/\partial t + J(\Psi_1, Q_1) = \kappa_T(\Psi_1 - \Psi_2)/(2\lambda^2) - \nu\nabla^6\Psi_1 + R_1,$$

$$\partial Q_2/\partial t + J(\Psi_2, Q_2) = -\kappa_T(\Psi_1 - \Psi_2)/(2\lambda^2) - \kappa_M\nabla^2\Psi_2 - \nu\nabla^6\Psi_2 + R_2, \quad (1)$$

where the potential vorticity Q_j is

$$Q_j = \beta y + \nabla^2\Psi_j + (-1)^j(\Psi_1 - \Psi_2)/(2\lambda^2),$$

and R_j is a time-independent forcing function.

The eddy streamfunctions ψ_i are now defined as departures from a state with a spatially uniform vertical shear of the zonal wind, with no meridional wind, and with the lower layer taken (for simplicity) at rest:

$$\Psi_1(x, y, t) = -U_0 y + \psi_1(x, y, t);$$

$$\Psi_2(x, y, t) = \psi_2(x, y, t). \quad (2)$$

We assume $U_0 > 0$, and non-dimensionalize (x, y, t, ψ_j) with $(\lambda, \lambda, \lambda/U_0, U_0\lambda)$, so that the dimensionless parameters are $\beta^* = \beta\lambda^2/U_0$, $(\kappa_M^*, \kappa_T^*) = (\kappa_M, \kappa_T)\lambda/U_0$, and $\nu^* = \nu/(U_0\lambda^3)$. Our motivation for non-dimensionalizing meridional as well as zonal distance by λ has been discussed in the introduction. In what follows, we omit the asterisks and assume all quantities are nondimensional unless otherwise stated. The transient eddy equations become

$$\partial q_j/\partial t + J(\psi_j, q_j) = F_j + D_j. \quad (3)$$

In (3), defining $\hat{\psi} = (\psi_1 - \psi_2)/2$, the transient potential vorticities are given by

$$q_j = \nabla^2\psi_j + (-1)^j\hat{\psi},$$

the terms describing the interaction with the time-mean flow by

$$F_1 = -\partial q_1/\partial x - (\beta + 1/2)\partial\psi_1/\partial x,$$

$$F_2 = -(\beta - 1/2)\partial\psi_2/\partial x,$$

and the nonconservative terms by

$$D_1 = \kappa_T\hat{\psi} - \nu\nabla^6\psi_1,$$

$$D_2 = -\kappa_T\hat{\psi} - \kappa_M\nabla^2\psi_2 - \nu\nabla^6\psi_2.$$

Aside from the inclusion of the radiative damping term, these are just the equations used in HH. We include radiative damping here for cleaner comparison with the channel model, where radiative damping is an essential aspect of the forcing.

The ψ_j are now assumed to consist of a zonally averaged part plus one nonzero zonal wavenumber:

$$\psi_j(x, y, t) = \psi_{j,0}(y, t) + (\psi_{j,k}(y, t)e^{ikx} + \text{c.c.}). \quad (4)$$

The first term on the right-hand side is referred to as the "zonal mean component" of the flow and the second term as the "wave component". Ignoring wave–wave interactions, the resulting equations of motion are

$$\partial q_{j,0}/\partial t = -2\,\mathrm{Re}\partial(v_{j,k}q^*_{j,k})/\partial y + F_{j,0} + D_{j,0}$$

$$\partial q_{k,j}/\partial t = ik(q_{k,j}\partial\psi_{j,0}/\partial y - \psi_{j,k}\partial q_{j,0}/\partial y) + F_{j,k} + D_{j,k},$$

where the decomposition of q, F and D terms is as in (4) and an asterisk denotes complex conjugation.

We now assume solutions to be of period $2\pi L$ in y, having the spectral decomposition

$$\psi_{j,m} = \sum_{n=-N+1,N} \psi_{j,m,n}(t)e^{il_n y}, \quad (5)$$

where $l_n = n/L$, m is either 0 or k, and $\psi_{j,0,0} = 0$. Since $\psi_{j,0}$ is real, $\psi_{j,0,-n} = \psi^*_{j,0,n}$ for $|n| < N$. With a given choice of L, the spectral resolution is $1/L$ and the maximum wavenumber retained is N/L; unless otherwise indicated, the experiments described here are conducted with $N = 256$. The resulting system of ordinary differential equations for the coefficients $\psi_{j,0,n}(t)$ and $\psi_{j,k,n}(t)$ is integrated with a combination of an explicit leapfrog scheme for the non-dissipative terms and a centered implicit scheme for the dissipative ones. To suppresss the computational mode, one of the two time levels of the leapfrog is discarded every 50 steps, and the integration restarted with a second-order accurate forward step. The Jacobians are computed using the alias-free transform method (Orszag 1971) in the meridional direction. Time integrations extend 1600 nondimensional time units, typically coming to statistical equilibrium in the first 200–400 time units, and time averages of statistics were taken over the period 600–1600. No exhaustive attempt was made to demonstrate the independence of the statistically steady states from the initial conditions, although no suggestions of nonuniqueness were found either. As indicated in section 4, very long time scales can be present in the integrations.

The steady-state energy and potential enstrophy budgets are derived by multiplying Eqs. (2.3)–(2.6) by streamfunction and potential vorticity and averaging in space and time as usual. Using angle brackets to denote horizontal averages, the vertically averaged total energy budget can be written

$$-\langle v_1 q_1\rangle/2 = \kappa_T\langle\hat{\psi}^2\rangle + \kappa_M\langle|\nabla\psi_2|^2\rangle/2 + \nu\langle|\nabla(\nabla^2\psi_1)|^2 + |\nabla(\nabla^2\psi_2)|^2\rangle/2,$$

where $v_1 = \psi_{1x}$. The term on the left-hand side is the energy generation term, and the terms on the right-hand side are the contributions to total dissipation made by (in order of appearance) thermal, Ekman, and diffusive damping.

The balances for potential enstrophy by layer, are

$$-\langle v_1 q_1\rangle(\beta + 1/2) = -\kappa_T\langle\hat{\psi}q_1\rangle + \nu\langle q_1\nabla^6\psi_1\rangle$$

$$-\langle v_2 q_2\rangle(\beta - 1/2) = -\kappa_T\langle\hat{\psi}q_2\rangle + \kappa_M\langle q_2\nabla^2\psi_2\rangle + \nu\langle q_2\nabla^6\psi_2\rangle.$$

Once again the generation term is on the left, the dissipative terms on the right.

All the generation terms are proportional to the potential vorticity flux in the upper layer; repeated integrations by parts show that

$$-\langle v_1 q_1\rangle = \langle v_2 q_2\rangle = -\langle\hat{\psi}(v_1 + v_2)/2\rangle, \quad (6)$$

the last term being proportional to the total meridional heat (or buoyancy) flux.

Spectra are calculated in the following manner. If the Fourier coefficients of $f(x, y)$ are F_{mn} (see Eq. 5), and those of $g(x, y)$ are G_{mn}, we define the spectrum $\{z_n\}$ of the zonal component of $\langle fg\rangle$ by

$$z_n = 2c_n\,\mathrm{Re}(F_{0,n}G^*_{0,n}), \quad n = 1, \cdots, N$$

and the spectrum $\{w_n\}$ of the wave component by

$$w_n = 2c_n\,\mathrm{Re}(F_{k,n}G^*_{k,n} + F_{k,-n}G^*_{k,-n}), \quad n = 0, \cdots, N$$

where c_n is ½, if $n = 0$ or $n = N$, and is 1, otherwise.

3. Statistically steady states of the doubly periodic model

In our units, the criterion for inviscid instability is $\beta < 0.5$, and the most unstable wavenumber is close to 0.7. All calculations in this paper will be with the fixed value for the wave component of $k = 0.7$. Before demonstrating the effects of varying other parameters, we discuss in some detail the equilibrated state for the particular choice of parameters $\beta = 0.15$, $\kappa_M = 0.3$, $\kappa_T = 0.067$, and $\nu = 0.001$. These values (the "comparison values") will be used in the next section for our closest examination of the asymptotic behavior of the channel model.

Figure 1 shows the linear growth rates as a function of meridional wavenumber l for this choice of β and k with (i) $\kappa_M = 0$, $\kappa_T = 0$; (ii) $\kappa_M = 0.3$, $\kappa_T = 0$; and (iii) $\kappa_M = 0.3$, $\kappa_T = 0.067$. The strong Ekman damping reduces the growth rates at $l = 0$ by nearly 40% and destabilizes short waves. The addition of thermal damping further reduces the strength of the instability by a modest amount. The growth rates are not affected significantly by the diffusion.

Figure 2 shows the meridional energy spectra for the wave and zonal mean components of the flow. Each figure shows results with three different values for the width of domain or, equivalently, the spectral resolution: $L = 20$, 40 and 80. (For the case $L = 80$, we increase the number of waves in the system to 512 so

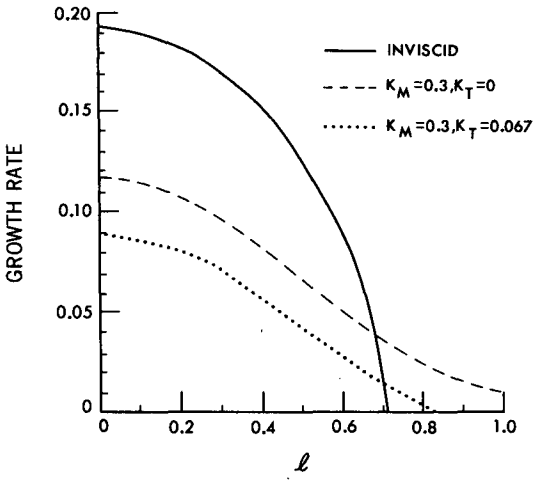

FIG. 1. Linear growth rates for doubly periodic model as a function of scaled meridional wavenumber: inviscid rates (solid); rates for $\kappa_M = 0.3$ and $\kappa_T = 0.0$ (dashed); and rates for $\kappa_M = 0.3$ and $\kappa_T = 0.067$ (dotted).

as to maintain resolution of the enstrophy dissipation.) Figure 3 shows the corresponding energy generation and nonlinear energy transfer spectra for the wave; the sum of these two terms is balanced by thermal and mechanical dissipation. A small amount of energy is transferred from the unstable waves to small meridional scales in the wave field, but the bulk of the nonlinear transfer is into the zonal mean flow. The spectrum of the nonlinear source of energy in the zonal mean flow (not shown) is very similar to the energy spectrum in Fig. 2.

If scales comparable to the width of the domain dominated the flow, there would be a spectral peak near $l = 0$ in the wave, and this peak would get narrower and higher as L and the spectral resolution increased. This would be in direct contradiction to our assumption on meridional scaling, but it clearly does not occur. The spectra have settled down even near $l = 0$. These results provide ample evidence that the statistics of the flow are insensitive to the width when this width is sufficiently large. Poor resolution in wavenumber space begins to make itself felt at $L \approx 10$. At this value, we find modest but significant differences from the results in the figure. For example, with $L = 10$ the wave energy at $l = 0$ is 0.9.

Holding the width of the domain fixed at $L = 20$, Fig. 4 shows how the domain-averaged eddy potential vorticity flux changes as the model parameters are varied about the comparison values. (The result for the comparison values is circled in each figure.) As noted

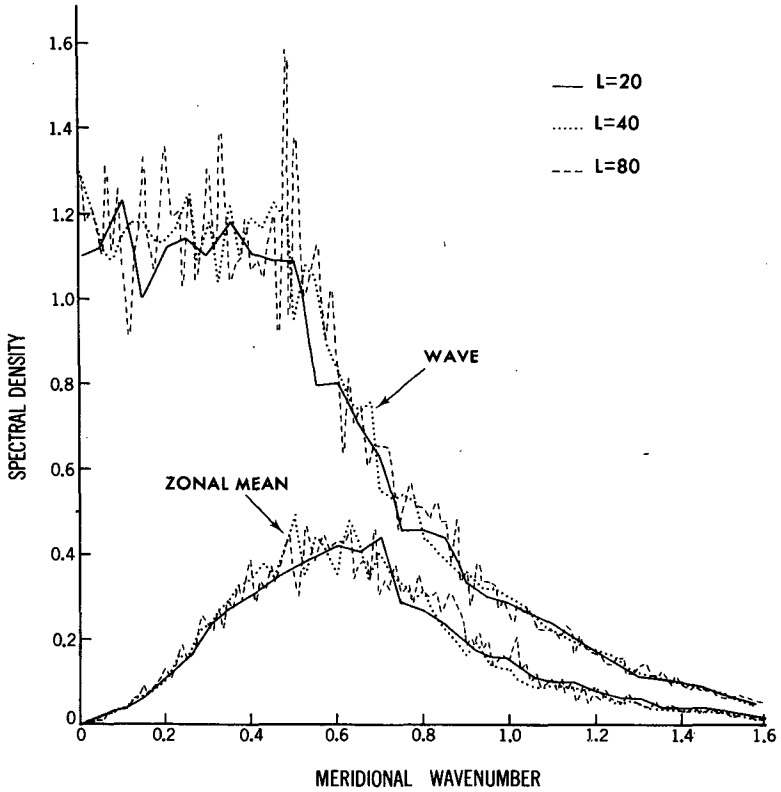

FIG. 2. Energy spectra for zonal mean and wave, for calculations with $L = 20$ (solid), 40 (dotted), and 80 (dashed). Parameters set at comparison values and averages taken over 1000 nondimensional time units after equilibration.

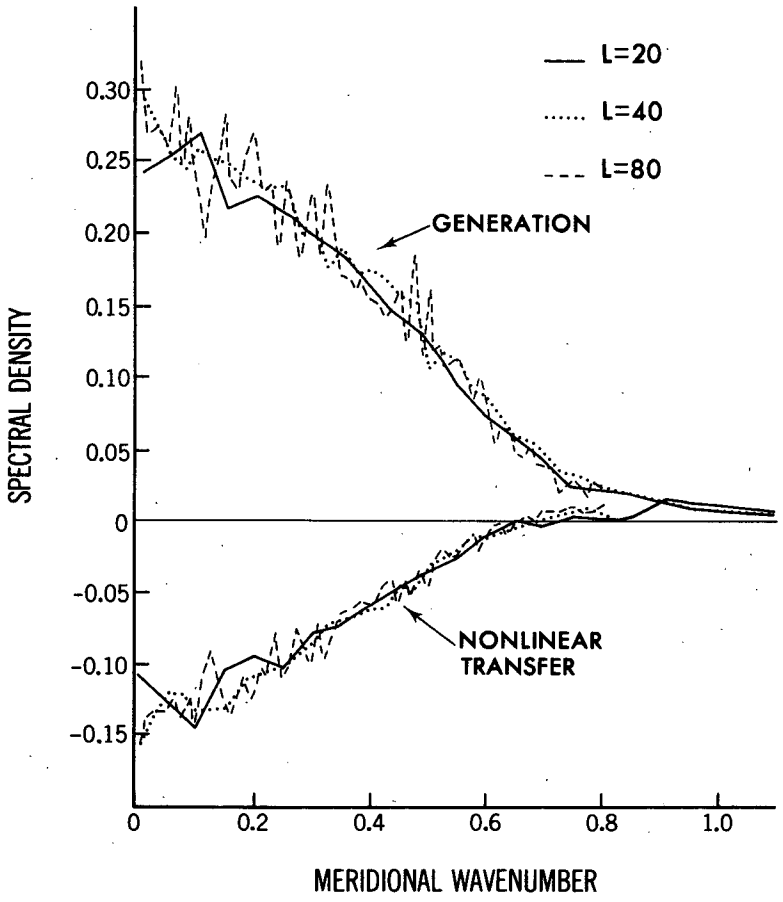

FIG. 3. Generation and transfer spectra for the wave component; curves and parameter values as in Fig. 2.

in (6), for this homogeneous system we may confine our attention to the upper layer flux.

Figure 4a shows how the flux varies as the biharmonic diffusion coefficient ν is varied. There exists a large range within which the flux is insensitive to the value of ν. Using the rms velocity U, of order unity in our calculations, an effective Reynold's number for the smallest scale in the model can be defined by $U/(\nu k_{\max})^3$ (Bennett and Haidvogel 1983). It is not until this number rises to values near 50 that the potential vorticity flux begins to decrease. (This distortion of the flux when the flow is not resolved is larger for smaller thermal damping.) For values of $\nu^{1/3}$ larger than 0.1, the flux begins to decrease again as the energy containing eddies begin to feel the diffusion.

Figure 4b shows that the flux increases monotonically as the strength of the thermal damping is decreased. The thermal damping has a significant effect on the flux even when it is much weaker than the Ekman friction and is too small to have a significant effect on linear growth rates (Fig. 1). The importance of small thermal damping is brought out by examining the fraction of dissipation due to each form of damping (Fig. 5). At our comparison value $\kappa_T = 1/15$, thermal damping accounts for 40% of the dissipation of energy and lower layer potential enstrophy, and 75% of the upper layer potential enstrophy dissipation. Biharmonic diffusion is significant only in the upper layer, where it is the only other nonconservative effect. The energy and lower layer potential enstrophy budgets continue to be dominated by Ekman and thermal damping until κ_T becomes extremely small; even in the upper layer, κ_T must be less than $1/50$ for diffusion to be competitive.

Biharmonic diffusion is a parametrization based only loosely on physical reasoning, so the relatively minor role it plays in these budgets is reassuring. But while diffusion accounts for a small fraction of the upper layer potential enstrophy dissipation for our comparison values, an enstrophy cascade still exists. Figure 6 shows the potential enstrophy spectrum in the upper layer for $\nu = 1 \times 10^{-3}$ and $\nu = 0$. Although the thermal damping prevents an inertial range from forming when $\nu = 1 \times 10^{-3}$, the flat enstrophy spectrum for $\nu = 0$ is clear evidence of a cascade.

Returning to Fig. 4, we see in Fig. 4c that the po-

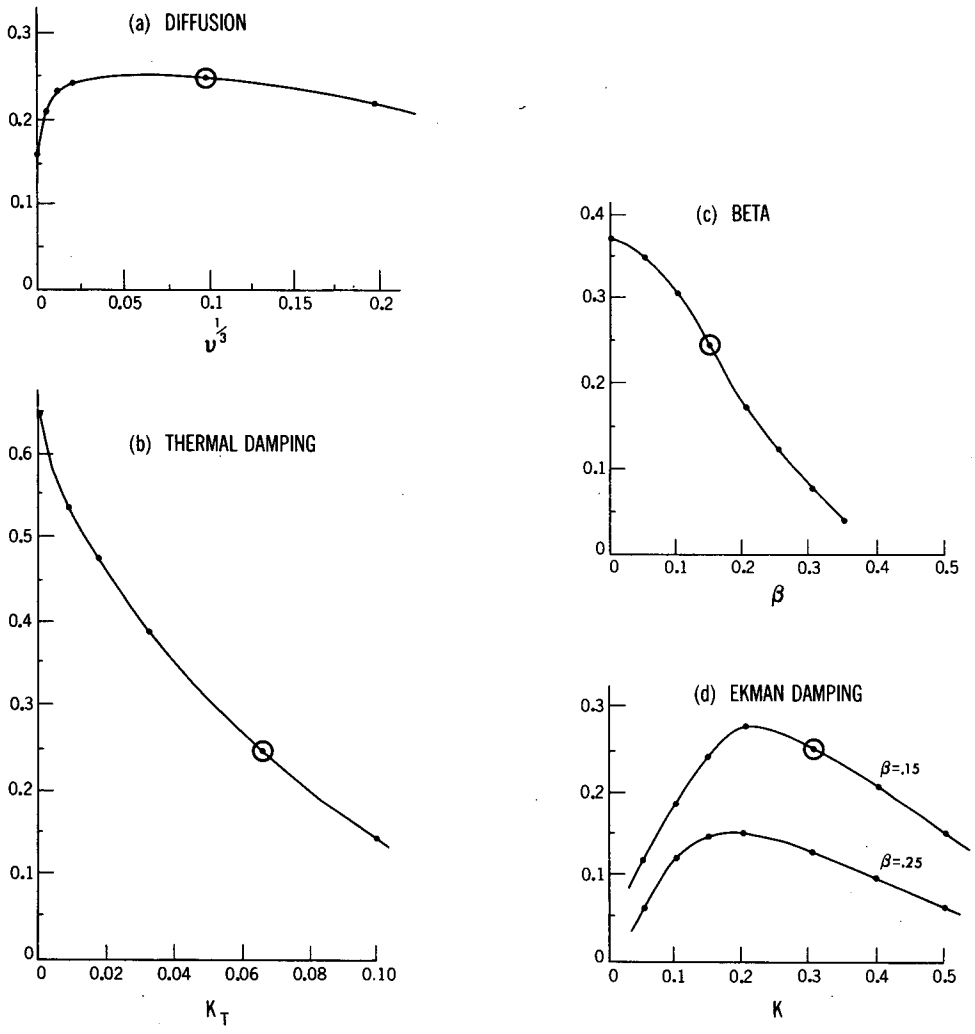

FIG. 4. Behavior of time-averaged $\langle -v_1 q_1 \rangle$ in doubly periodic model, for variations in one parameter with others fixed at comparison values: (a) diffusion; (b) thermal damping; (c) beta; and (d) Ekman damping, with a second curve showing results with β held at 0.25. In each figure, the circled dot denotes the comparison value.

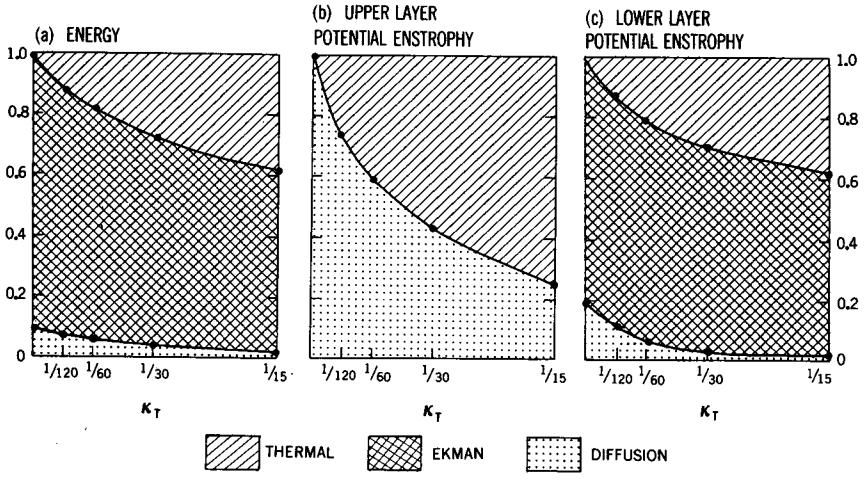

FIG. 5. For doubly periodic model, fractional contributions of each dissipative process in time-averaged budgets of (a) energy, (b) upper-layer potential enstrophy, and (c) lower layer potential enstrophy.

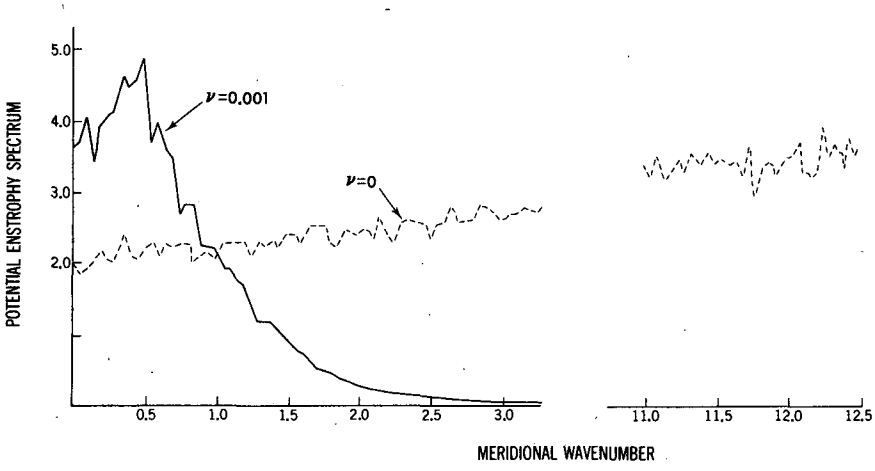

FIG. 6. Upper-layer potential enstrophy spectrum in doubly periodic model, with and without biharmonic diffusion (other parameters at their comparison values).

tential vorticity flux increases monotonically with decreasing β, as anticipated. More surprisingly, the dependence on κ_M is not monotonic (3d), reaching a maximum value at $\kappa_M \approx 0.2$. For smaller values of κ_M, the flux appears to be roughly proportional to κ_M. We also show calculations with $\beta = 0.25$ which suggest that the value of κ_M at which the flux maximizes decreases with increasing β. The dynamics of this flow at small κ_M is very different from that in weakly nonlinear models in which the flux is also proportional to the strength of the damping; we suspect that the large amount of energy accumulating in the zonal mean component of the flow at small κ_M distorts the baroclinic eddies and reduces their transport (cf. Salmon 1980).

4. The channel model

The (nondimensional) equations for the channel model are given by

$$\partial Q_1/\partial t + J(\Psi_1, Q_1) = \kappa_T[(\Psi_1 - \Psi_2)/2 - \tau_e] - \nu\nabla^6\Psi_1,$$

$$\partial Q_2/\partial t + J(\Psi_2, Q_2) = -\kappa_T[(\Psi_1 - \Psi_2)/2 - \tau_e] - \kappa_M\nabla^2\Psi_2 - \nu\nabla^6\Psi_2. \quad (6)$$

No decomposition is made into the time-mean flow and transients. The system is now forced explicitly by linear relaxation to an unstable "radiative equilibrium temperature profile" or interface slope $\tau_e(y)$. The vertical shear in the absence of eddy potential vorticity fluxes is $U_e = -\partial\tau_e/\partial y$. The form we choose for U_e is

$$U_e = \frac{1}{2}\begin{cases} U_0, & |y| < W \\ U_0 \exp(-[(y - W)/\sigma]^2), & |y| > W. \end{cases} \quad (7)$$

The radiative equilibrium winds are flat in a central region of width $2W$ and then decay to zero exponentially outside of this region (see Fig. 8a). The width W will be varied in the following, but we fix $\sigma = 4$. Since we think of the doubly periodic model as simulating the flow in the interior of such a channel, we set $U_0 = 1$, consistent with the nondimensionalization of the doubly periodic model in section 2. The width of the channel is taken to be 100 radii of deformation, which will always be large enough that we can think of U_e as being zero at the walls.

The streamfunction Ψ_j is once again decomposed into the zonal mean flow plus one nonzero zonal wavenumber, and wave–wave interactions are ignored. The streamfunction for the wave must vanish at the channel boundaries: $\Psi_{j,k} = 0$ at $y = \pm L/2$. For the biharmonic diffusion, we choose the boundary conditions $\partial\zeta/\partial y = \partial^3\zeta/\partial^3 y = 0$ for both wave and zonal mean. Since the eddy activity is confined to the center of the channel in all of the calculations described here, the choice of this boundary condition should have no significant effects on the eddy statistics. At the boundaries, the zonal mean flow must also satisfy

$$\partial U_1/\partial t = 0; \quad \partial U_2/\partial t = -\kappa U_2,$$

where $U_j = -\partial\Psi_{j,0}/\partial y$. We always start with the initial conditions $U_j = 0$, so we can take $U_j = 0$ as the boundary condition also. We use standard centered-differencing for relating the vorticity and streamfunction and in evaluating the diffusion. The resulting equations conserve analogs of both energy and enstrophy when the nonconservative terms are omitted. The number of meridional grid points is 1000.

Before considering the structure of the equilibrated flow, we present in Fig. 7a an example of the spinup of the channel model when the width of the unstable region is much larger than the radius of deformation [$W = 40$ in Eq. (7); other parameters are given their comparison values]. Plotted in the figure is the squared

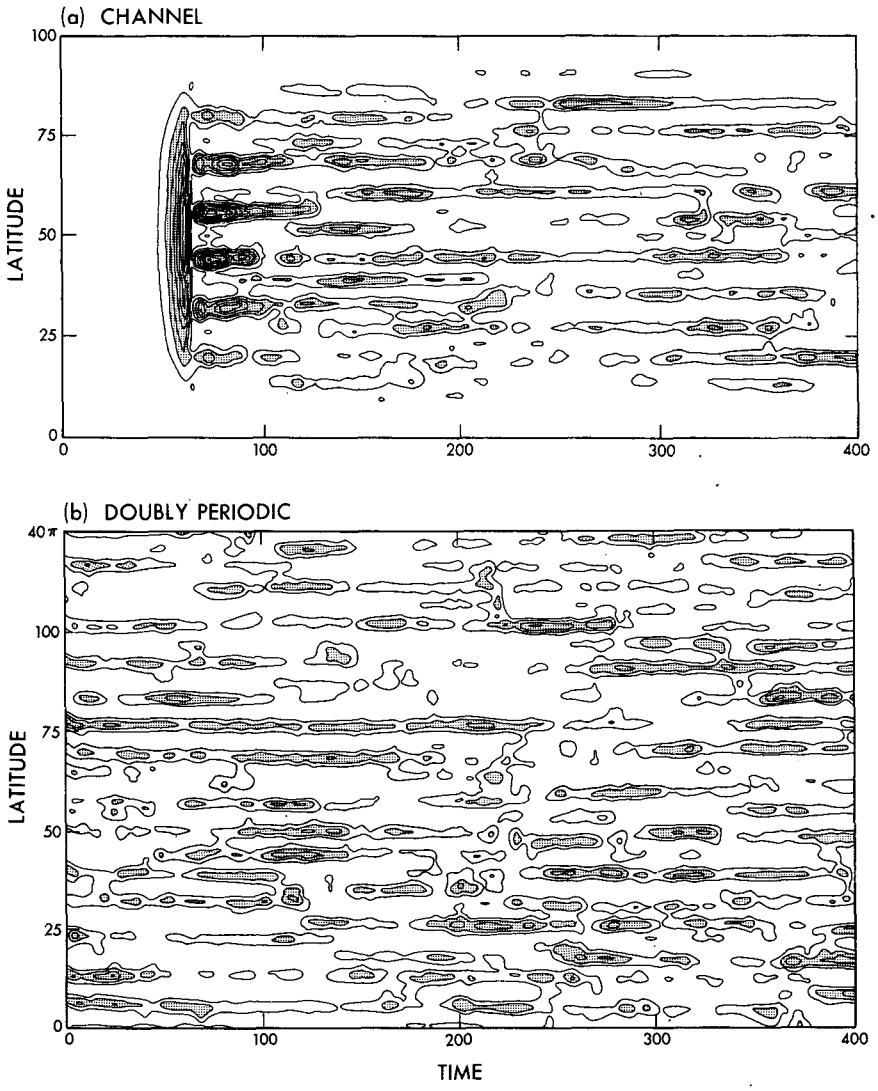

FIG. 7. Zonally averaged upper-layer streamfunction amplitude (squared) as a function of nondimensional time and meridional distance. Panel (a) shows spinup in the channel model with $W = 40$; (b) shows 400 time-unit sample from doubly periodic model.

upper-layer streamfunction amplitude, zonally averaged, as a function of y and t. The initial condition has a small barotropic eddy streamfunction [$\propto \sin(\pi y/L)$], where L is the width of the channel, on a zonally averaged flow in radiative equilibrium. The initial emergence of the gravest cross-stream mode is clear. Equally clear is the rapid transition to structures with smaller meridional scales. The flow evolves into a multiple storm track structure. The evolution within each storm track is chaotic, and the interactions between distinct storm tracks weak. Each storm track is associated with a zonal wind maximum in both the upper and lower layers. Once formed, there is surprisingly little tendency for an existing jet and its associated stormtrack to move to a different latitude. Instead, they seem to decay in place and then are regenerated at a different location. The meridional structure generated by the initial instability of the gravest mode is not an accurate predictor of the number of jets, or storm tracks, in the equilibrated flow. Also, the amplitude attained by the gravest mode in its initial growth, during which time it can draw on the available potential energy in the entire unstable region, is typically far in excess of the statistically steady eddy amplitudes.

We are arguing that the doubly periodic model should reproduce the statistical behaviour of the channel's interior region at equilibrium. Figure 7b is a 400 time unit sample (after equilibration) of the time evolution of the squared upper-layer eddy streamfunction amplitude in the doubly periodic model, and can be

directly compared to the channel model result in 7a. The parameters are set at their comparison values. The qualitative similarity of the two flows is evident; notice especially that the figures use the same meridional scales.

Figure 8 shows the time- and zonally averaged winds, potential vorticity gradients, and potential vorticity fluxes for channel half-widths W equal to 5, 10, 20 and 40, with all parameters at their comparison values. The time-averaging period in each case is the final 1000 of a 1600 time unit integration. The multiple jet structures that form when W is large are difficult to eliminate by time-averaging. Given the long time scales evident in Fig. 7, we cannot be sure how much of this structure would disappear if the length of the averaging period were increased. The amount of asymmetry about the center of the channel can presumably be taken as a measure of the sampling error.

The contrast in the structure of the upper and lower potential vorticity fluxes is striking. The upper layer flux shows little or no meridional structure on the scale of the jets. Zonal averages taken using the doubly periodic model show the same multiple jet structures and the same qualitative difference between the potential vorticity fluxes in the two layers. The relation between the structure of the fluxes and that of the jets is determined by the relative strengths of the mechanical and thermal damping. Consider the zonally averaged potential vorticity equations, once differentiated in the meridional direction:

$$\partial^2/\partial y^2(\overline{v_1 q_1}) = -\kappa_T \hat{U}(y) + \nu\partial^6/\partial y^6 \bar{U}_1$$

$$\partial^2/\partial y^2(\overline{v_2 q_2}) = \kappa_T \hat{U}(y) + \kappa_M \partial^2/\partial y^2 \bar{U}_2 + \nu\partial^6/\partial y^6 \bar{U}_2, \tag{8}$$

where $\hat{U}(y)$ is the zonally and time averaged eddy shear in the zonal wind (defined according to Eq. (1) or (6)). Assume that the biharmonic diffusion makes an insignificant contribution to this mean-flow budget. Suppose further that $\hat{U}$, U_2, and $\overline{v_i q_i}$ each consist of a part that varies slowly, on the scale of the forcing, and a part ($\hat{U}^J$, ${U_2}^J$, $\overline{v_i q_i}^J$) varying more rapidly like $\sin(ly)$, where l^{-1} is the meridional scale of the jets. The jets are observed to be equivalent barotropic, so we make the approximation $\hat{U}^J \approx \alpha {U_2}^J$, and approximate (8) by

$$\overline{v_1 q_1}^J \approx l^{-2}\kappa_T \hat{U}^J \approx \alpha l^{-2}\kappa_T {U_2}^J$$

$$\overline{v_2 q_2}^J \approx -l^{-2}\kappa_T \hat{U}^J + \kappa_M {U_2}^J \approx (\kappa_M - \alpha l^{-2}\kappa_T){U_2}^J \tag{9}$$

For the calculations in Fig. 8, $\alpha l^{-2}\kappa_T \ll \kappa_M < 1$, hence the lower layer flux has the structure of the jets, and the upper layer flux is essentially flat ($\overline{v_1 q_1}^J \approx 0$). We have no theory for how α might depend on external parameters, but Eq. (9) suggests that as κ_T increases, the upper layer flux will begin to show jetlike structure. Calculations using larger values of thermal damping show this to be the case.

The time–mean potential vorticity gradients for the channel model in Fig. 8 make it plain that for $W > 10$ (at this parameter setting), the eddies are incapable of significantly reducing the negative gradient in the lower layer. This behavior is in sharp contrast to that assumed in the simplest "baroclinic adjustment" hypothesis (Stone 1972) in which the potential vorticity fluxes are assumed to be those needed to restore the gradient in the lower layer to zero. This hypothesis requires the flux to increase with the square of the width of the unstable region, which is totally at variance with the behavior of the channel model, even for a half-width W of 5 Rossby radii.

The zonally averaged zonal winds, potential vorticity fluxes, and potential vorticity gradients for the doubly periodic model (not shown here) would be just as hard to distinguish from corresponding channel interior statistics in Fig. 8, when $W = 40$, as was the case for streamfunction amplitude in Fig. 7.

Figure 9 shows the approach of the upper layer potential vorticity flux to a limiting value in the channel model as the half-width W increases. To decrease the sampling error, advantage has been taken of the model's symmetry about $y = 0$ by averaging flux values at $+y$ and $-y$. The solid horizontal line, labeled "homogeneous limit," is the prediction of the periodic model with the same parameters. Granted some uncertainty in the time averages, the fluxes in the central region are seen to be asymptotic to a value very close to the periodic model's prediction.

The fact that the solutions for $W = 20$ and $W = 40$ in Fig. 9 are closer to each other in the center of the channel than either is to the homogeneous limit should not be taken as evidence of a significant bias in the doubly periodic model. In Fig. 10 we compare the prediction of the doubly periodic model with the meridional behavior of the time-averaged flux in the channel model for different values of β. The other parameters are given their comparison values, with $W = 20$. There is no consistent tendency for the doubly periodic model to over- or under-predict the channel model's flux. The dependence of the flux on β is clearly similar in the two models. The sampling errors in the fluxes are evidently 15% or so. An attempt to clearly define the difference between the flux behavior in the two models would require much longer integrations of the channel model than were used for this study.

5. Discussion and conclusions

Forcing a quasi-geostrophic model in a channel by radiative relaxation to an unstable temperature gradient, we have demonstrated that the eddy statistics asymptote to limiting values as the width of the uniformly unstable region is increased. Furthermore, the limiting behavior is the same as that produced in a

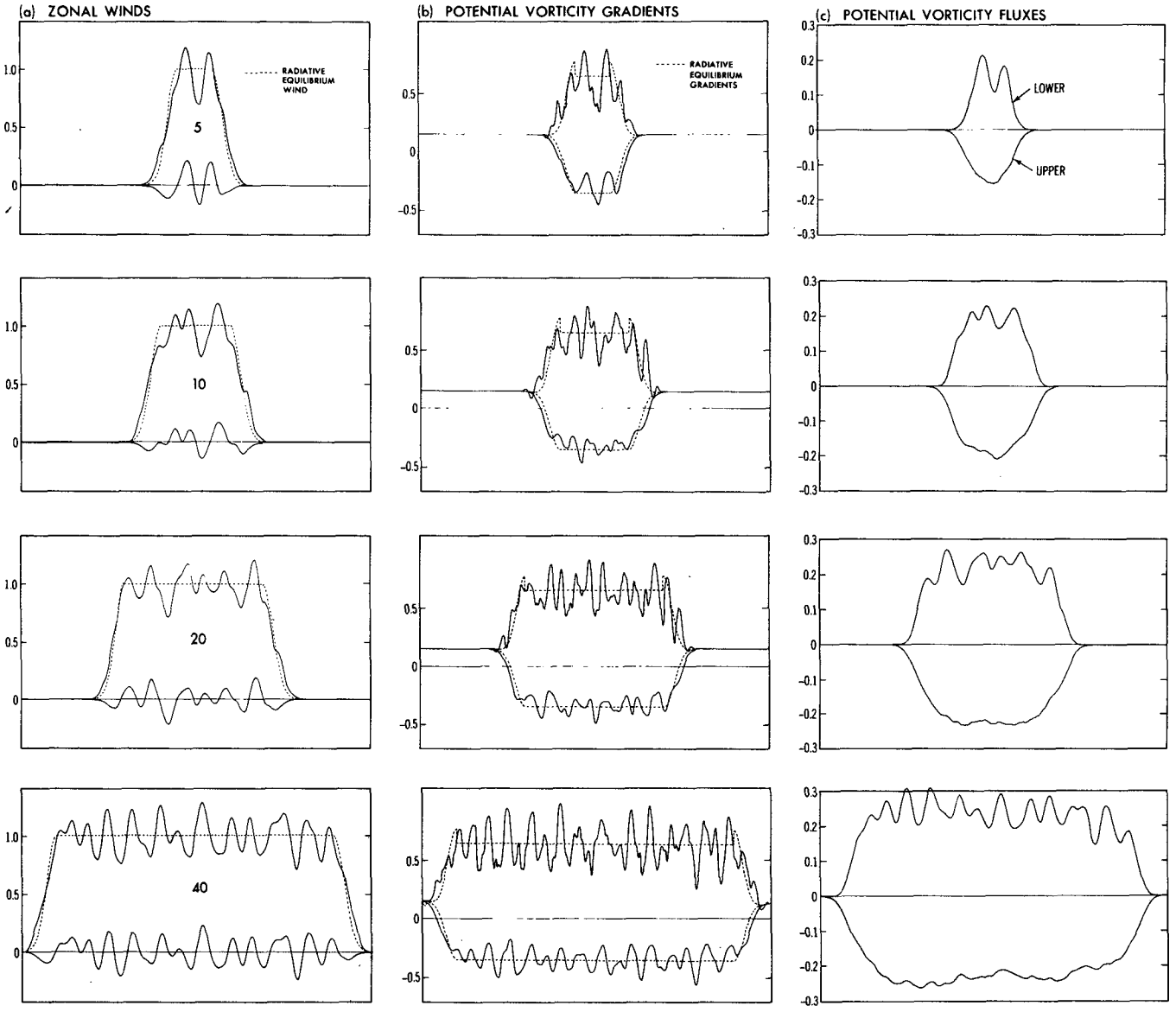

FIG. 8. Channel model: meridional structure of time averaged (a) zonal winds, (b) potential vorticity gradients, and (c) potential vorticity fluxes, for values of $W = 5, 10, 20, 40$. Except in (c), upper (lower) curves are upper (lower) layer values, and radiative relaxation profiles are indicated by dashed curves. Half-widths are indicated in (a).

doubly periodic model in which the spatially averaged time mean flow is fixed and the transients are assumed to be periodic in latitude as well as longitude. While we have used a two-layer model truncated to one nonzero zonal wavenumber (plus the zonal flow) to make this point, we see no compelling reason to suspect that this limit does not also exist in models that are untruncated in the vertical and zonal dimensions.

In his study of a similar doubly periodic model, Salmon (1980) forces the time mean flow [U_0 in our Eq. (2)] to vary so as to maintain the domain-averaged eddy energy generation at a specified value; in effect he fixes the potential vorticity flux and solves for the shear. We have demonstrated that this kind of modification of the governing equations is not necessary. Aside from this we see our work as being complementary to his. Having demonstrated the physical significance of the doubly periodic model, one is now justified in pursuing detailed closure schemes (such as Salmon 1980) for homogeneous turbulence that would help explain behavior in the model.

The very existence of a limiting value for eddy po-

tential vorticity fluxes means that any adjustment theory which requires eddies to neutralize the flow by destroying the reversed potential vorticity gradients in the lower layer (or reducing them by a certain amount) must become invalid for a sufficiently wide unstable region; otherwise the fluxes would have to increase without bound. As predicted by the doubly periodic model, both here and in Salmon (1980), the time averaged flow remains strongly supercritical. Only when the radiative relaxation is sufficiently weak, or the unstable region is sufficiently narrow, do we find significant neutralization by the eddies, as in Fig. 8 for $W = 5$.

One can test whether neutralization is to be expected by the following check: assume that the limiting value of the potential vorticity flux for a wide unstable region is relevant *at each latitude,* using the local value of the radiative equilibrium shear; compute the mean flow modification due to the resulting latitude-dependent potential vorticity flux (this modification will be inversely proportional to the strength of the radiative relaxation of the mean flow, κ_T); if this is negligible, the limiting case is self-consistent and neutralization should not occur. If significant mean flow modification is expected, one can attempt to estimate it by this local theory even if it is not strictly justified. Preliminary attempts along these lines suggest that such a calculation can be qualitatively useful. Just as many asymptotic expansions can be useful even when the expansion parameter is of order unity, we suspect that the relevance of the wide-channel limit of the potential vorticity flux is not limited to very wide channels.

The multiple jets and storm tracks that form in wide unstable regions complicate this picture by introducing very long time scales and the possibility of inhomogeneity even in wide channels. On the one hand, if the statistically steady state of the doubly periodic model is unique (as we believe), the homogeneity of the forcing implies that any quantity averaged over a sufficiently long period will also be spatially homogeneous. On the other hand, the extent to which the multiple jets average out in the channel model is uncertain. Whether or not they do migrate sufficiently so as to produce homogeneous statistics in the interior, we do not think that there would be large changes in the eddy fluxes averaged over scales larger than that of the jets; that is, we anticipate that the upper-layer potential vorticity flux would not change appreciably, while the meridional structure of lower layer flux would come to resemble the upper layer flux more closely. Notice that only on such a long time scale would any simple "K-theory" correctly predict the relation between the flux and gradient of potential vorticity in the upper layer.

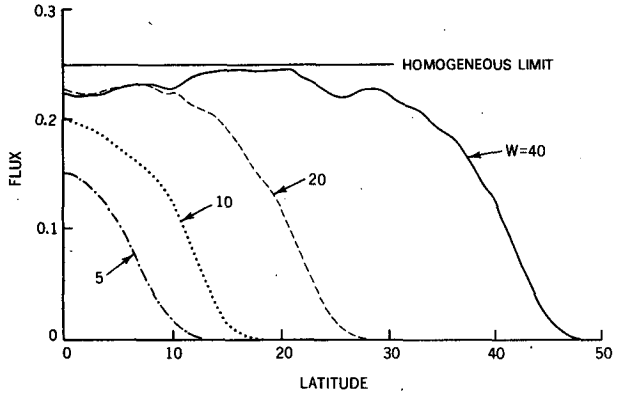

FIG. 9. The approach of time-averaged $-\overline{v_1 q_1}(y)$ in channel model to the value predicted by the doubly periodic model (the homogeneous limit) as the unstable region is widened ($W = 5, 10, 20, 40$).

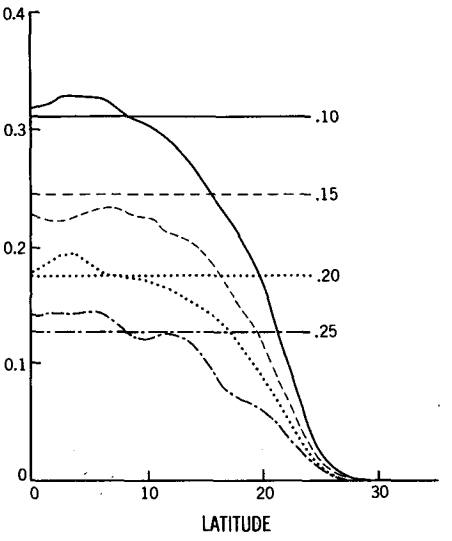

FIG. 10. For fixed $W = 20$, comparison of $-\overline{v_1 q_1}(y)$ in channel model with the corresponding homogeneous limit, for $\beta = 0.10$ (solid curves), 0.15 (dashed), 0.20 (dotted), and 0.25 (dash-dotted).

One expects some modification of the jets when the severe zonal truncation is relaxed, since a jet of a given scale can be stable to the retained wavenumber k but unstable to longer waves. But as long as β is nonzero, we expect (following Rhines 1975) some long-lived jets to be a part of the statistics of wide unstable regions. Such regions occur, for example, in recirculation regions of oceanic subtropical gyres; Yoshida (1970) reported zonal jets in data taken from the North Pacific, and Cox (1987) found similar behavior in his oceanic GCM. Calculations with an isotropically truncated doubly periodic model (which will be reported elsewhere) show that the jets are not a feature special to the zonally truncated model.

Acknowledgments. One of us (R.L.P.) was supported during the course of this work by NOAA Grants 04-07-022-44017 and NA85ABH00031.

REFERENCES

Bennett, A. F., and D. B. Haidvogel, 1983: Low resolution numerical simulation of decaying two-dimensional turbulence. *J. Atmos. Sci.*, **40,** 738–748.

Cox, M. D., 1987: An eddy-resolving numerical model of the ventilated thermocline: Time dependence. *J. Phys. Oceanogr.*, **17,** 1044–1056.

Geisler, J. E., and R. E. Dickinson, 1974: Numerical study of an interacting Rossby wave and barotropic zonal flow near a critical level. *J. Atmos. Sci.*, **31,** 946–955.

Haidvogel, D. B., and I. M. Held, 1980: Homogeneous quasi-geostrophic turbulence driven by a uniform temperature gradient. *J. Atmos. Sci.*, **37,** 2644–2660.

Haynes, P. H., and M. E. McIntyre, 1986: On the representation of planetary-wave critical layers and wave-breaking in zonally truncated models. *J. Atmos. Sci.*, **44,** 2381–2404.

Held, I. M., and M. J. Suarez, 1980: A two-level primitive equation atmospheric model designed for climate sensitivity experiments. *J. Atmos. Sci.*, **35,** 206–229.

Holton, J. R., 1971: A semi-spectral numerical model of wave–mean flow interactions in the stratosphere: Application to sudden stratospheric warmings. *J. Atmos. Sci.*, **33,** 1639–1649.

McWilliams, J. C., 1984: The emergence of isolated coherent vortices in turbulent flow. *J. Fluid Mech.*, **146,** 21–43.

Matsuno, T., 1971: A dynamical model of the sudden stratospheric warming. *J. Atmos. Sci.*, **28,** 1479–1494.

Orszag, S. A., 1971: Numerical simulation of incompressible flows within simple boundaries. I. Galerkin (spectral) representations. *Stud. Appl. Math.*, **50,** 293–327.

Pedlosky, J., 1975: On secondary baroclinic instability and the meridional scale of motion in the ocean. *J. Phys. Oceanogr.*, **5,** 603–607.

Rhines, P. B., 1975: Waves and turbulence on a beta plane. *J. Fluid Mech.*, **69,** 417–443.

Salmon, R., 1980: Baroclinic instability and geostrophic turbulence. *Geophys. Astrophys. Fluid Dyn.*, **15,** 167–211.

Stone, P. H., 1972: Baroclinic adjustment. *J. Atmos. Sci.*, **35,** 561–571.

Yoshida, K., 1970: Subtropical countercurrents: Band structures revealed from CSK data. *The Kuroshio,* J. C. Marr, Ed., East-West Center Press, 197–204.